JOURNAL OF MULTIFUNCTIONAL MATERIALS & PHOTOSCIENCE
11(1), June 2020, pp. 37-45

Microwave Sol-Gel Derived Synthesis of $Ho^{3+}/Yb^{3+}/Tm^{3+}$ Tri-doped $NaGd(WO_4)_2$ Phosphors and Their Spectroscopic Properties

Won-Chun Oh, Hak Su Kim, Ki Soo Lee, Chang Sung Lim*
Department of Aerospace Advanced Materials & Chemical Engineering, Hanseo University, Seosan Haemimyeon 31962, Republic of Korea
Corresponding author: cslim@hanseo.ac.kr

Abstract: Microwave sol-gel derived (MSG) Ho3+/Yb3+/Tm3+ tri-doped NaGd1-x(WO4)2 white phosphors were successfully synthesized with variations of Ho3+, Yb3+ and Tm3+ (x = Ho3+ + Yb3+ + Tm3+, Ho3+ = 0.04, 0.03, 0.02, 0.01, Yb3+ = 0.35, 0.40, 0.45, 0.50 and Tm3+ = 0.01, 0.02, 0.03, 0.04), and their spectroscopic properties were evaluated. The synthesized particles have been fairly crystallized and showed a superior microcrystalline morphology with particle sizes of 1-2 μm. The spectroscopic properties were examined comparatively using photoluminescence emission and Raman spectroscopy. Under excitation at 980 nm, the doped particles exhibited white emissions based on blue, green and red emission bands, which correspond to the 1G4 ? 3H6 transitions of Tm3+ in the blue region, the 5S2/ 5F4 ? 5I8 transitions of Ho3+ in the green region, the 5F5 ? 5I8 transitions of Ho3+ as well as the 1G4 ? 3F4 and 3H4 ? 3H6 transitions of Tm3+ in the red region. The pump power dependence was provided, and the individual chromacities corresponding to the equal points in the CIE diagram revealed white emissions.

Keywords: Microwave sol-gel, Phosphors, White emission, Spectroscopic, Raman spectroscopy.

1. Introduction

Scheelite-structured compounds belonging to the tungstates family have been interested and attracted great application due to their unique spectroscopic properties and dramatically excellent upconverted (UC) optical properties [1]. These UC characteristics of the scheelite-structured compounds have current applications in many fields, including optoelectronic devices and luminescence imaging, due to their excellent UC luminescencent behaviors. They could overcome the present limitations and enhance the applications of the traditional photoluminescence (PL) materials [2,3]. In particular, rare-earth doped binary $NaLn(WO_4)_2$ (Ln = Gd^{3+}, Y^{3+} and La^{3+}) compounds belong to the space group $I4_1/a$ with the tetragonal phase, and have the family of scheelite-type structure [4,5]. The trivalent lanthanide ions are partially substituted into the crystalline lattices of the tetragonal double tungstate crystal phase. The available doping could be attributed to the very similar radii of the trivalent lanthanide ions and bring to the

excellent properties for UC PL[6]. Multicolor and white light emissions can be generated via tri-doping system based on blue, green and red emission bands. Many lanthanide doping materials such as laser active Ho^{3+} and Tm^{3+} are employed as an activator in luminescent centers for Yb^{3+} as a sensitizer, because their unique electronic energy levels. The tri-doped Yb^{3+}, Ho^{3+} and Tm^{3+} ions can remarkably enhance the UC efficiency for the shift from infrared to visible light due to the efficiency of the energy transfer from Yb^{3+} to Ho^{3+} and Yb^{3+} to Tm^{3+}. Ho^{3+} exhibits $^5S_2/\ ^5F_4$ '! $^5I_8$ transitions in the green region, $^5F_5$ '! $^5I_8$ transitions in the red region in UC process, while Tm^{3+} shows the $^1G_4$ '! $^3H_6$ transitions in the blue region, and $^1G_4$ '! $^3F_4$ and $^3H_4$ '! $^3H_6$ transitions in the red region [7-9]. These ions are effectively doped into the crystal lattices of the tetragonal phase due to the similar radii of the trivalent rare-earth ions, these results in high red emitting efficiency, and superior thermal and chemical stability in white emitting diode.

$NaLn(WO_4)_2$(Ln = Gd^{3+}, Y^{3+} and La^{3+}) phosphors have been synthesized via specific preparation processes [10-15]. Compared with the above methods, microwave synthesis has the advantages of a very short reaction time, small-size particles, narrow particle size distribution, and high purity of final polycrystalline samples [16]. A microwave sol-gel (MSG) derived process provides high homogeneity, and brings a unique alternative approach for the available synthesis of high-quality PL materials. However, the synthesis of $Ho^{3+}/Yb^{3+}/Tm^{3+}$ tri-doped $NaGd(WO_4)_2$ (NGW) phosphors via the MSG route has not been reported. In this study, the double tungstate NGW phosphors with the proper doping concentrations of Ho^{3+}, Yb^{3+} and Tm^{3+} (x = Ho^{3+} + Yb^{3+} + Tm^{3+}, Ho^{3+} = 0.04, 0.03, 0.02, 0.01, Yb^{3+} = 0.35, 0.40, 0.45, 0.50 and Tm^{3+} = 0.01, 0.02, 0.03, 0.04) were successfully prepared by the MSG derived method, followed by heat treatment. The synthesized particles were characterized by X-ray diffraction (XRD) and scanning electron microscopy (SEM). The pump power dependence of the UC emission intensity and Commission Internationale de L'Eclairage (CIE) chromatic coordinates were evaluated in detail. The spectroscopic properties were examined comparatively using photoluminescence (PL) emission and Raman spectroscopy.

Experimental

Precise stoichiometric amounts of Na_2WO_4'"$2H_2O$ (99 %, Sigma-Aldrich, USA), $Gd(NO_3)_3$'"$6H_2O$ (99 %, Sigma-Aldrich, USA), $(NH_4)_6W_{12}O_{39}$'"xH_2O (99%, Alfa Aesar, USA), $Ho(NO_3)_3$'"$5H_2O$ (99.9%, Sigma-Aldrich, USA), $Yb(NO_3)_3$'"$5H_2O$ (99.9%, Sigma-Aldrich, USA), $Tm(NO_3)_3$'"$5H_2O$ (99.9%, Sigma-Aldrich, USA), citric acid (99.5%, Daejung Chemicals, Korea), NH_4OH (A.R.), ethylene glycol (A.R.) and distilled water were used to prepare then compounds. To prepare $NaGd_{0.60}(WO_4)_2$:$Ho_{0.04}/Yb_{0.35}/Tm_{0.01,}$ 0.2 mol% Na_2WO_4'"$2H_2O$ and 0.067 mol% $(NH_4)_6W_{12}O_{39}$'"xH_2O were dissolved in 20 mL of ethylene glycol and 80 mL of 5M NH_4OH under vigorous stirring and heating. Subsequently, 0.24 mol% $Gd(NO_3)_3$'"$6H_2O$ with 0.016 mol% $Ho(NO_3)_3$'"$5H_2O$, 0.14 mol% $Yb(NO_3)_3$'"$5H_2O$ and 0.004 mol% $Tm(NO_3)_3$'"$5H_2O$, and citric acid (with a molar ratio of citric acid to total metal ions of 2:1) were dissolved in 100 mL of distilled water under vigorous stirring and heating. Then, the solutions were mixed together under vigorous

stirring and heating at 80-100°C. Finally, highly transparent solutions were obtained and adjusted to pH=7-8 by the addition of 8M NH_4OH. In order to prepare $NaGd_{0.55}(WO_4)_2:Ho_{0.03}/Yb_{0.40}/Tm_{0.02,}$ the mixture of 0.22 mol% $Gd(NO_3)_3'''6H_2O$ with 0.012 mol% $Ho(NO_3)_3'''5H_2O$, 0.16 mol% $Yb(NO_3)_3'''5H_2O$ and 0.008 mol% $Tm(NO_3)_3'''5H_2O$ was used for the creation of the rare-earth solution. In order to prepare $NaGd_{0.50}(WO_4)_2:Ho_{0.02}/Yb_{0.45}/Tm_{0.03,}$ the mixture of 0.20 mol% $Gd(NO_3)_3'''6H_2O$ with 0.008 mol% $Ho(NO_3)_3'''5H_2O$, 0.18 mol% $Yb(NO_3)_3'''5H_2O$ and 0.012 mol% $Tm(NO_3)_3'''5H_2O$ was used for the creation of the rare-earth solution. In order to prepare $NaGd_{0.45}(WO_4)_2:Ho_{0.01}/Yb_{0.50}/Tm_{0.04,}$ the rare-earth containing solution was generated using 0.18 mol% $Gd(NO_3)_3'''6H_2O$ with 0.004 mol% $Ho(NO_3)_3'''5H_2O$, 0.20 mol% $Yb(NO_3)_3'''5H_2O$ and 0.016 mol% $Tm(NO_3)_3'''5H_2O$.

The MSG derived process has been previously reported in the references of [1,3,6,16]. The phase composition of the synthesized particles was identified using XRD (D/MAX 2200, Rigaku, Japan). The microstructure and surface morphology of the synthesized particles were observed using SEM (JSM-5600, JEOL, Japan). The PL spectra were recorded using a spectrophotometer (Perkin Elmer LS55, UK) at room temperature. Raman spectroscopy measurements were performed using a LabRam Aramis (Horiba Jobin-Yvon, France). The 514.5-nm line of an Ar ion laser was used as the excitation source, and the power on the samples was kept at 0.5 mW.

Results and Discussion

Fig. 1 shows the X-ray diffraction patterns of the (a) JCPDS 25-0829 data of NGW, the synthesized (b) $NaGd_{0.60}(WO_4)_2:Ho_{0.04}/Yb_{0.35}/Tm_{0.01,}$ (c) $NaGd_{0.55}(WO_4)_2:Ho_{0.03}/Yb_{0.40}/Tm_{0.02,}$ (d) $NaGd_{0.50}(WO_4)_2:Ho_{0.02}/Yb_{0.45}/Tm_{0.03}$, and (e) $NaGd_{0.45}(WO_4)_2:Ho_{0.01}/Yb_{0.50}/Tm_{0.04}$ particles. All of the XRD peaks could be assigned to the tetragonal-phase NGW with the space group of $I4_1/a$, which was in good agreement with the crystallographic data of NGW (JCPDS 25-0829). It is observed that the diffraction peaks of the doped samples in Fig. 1(b)-(e) shift slightly to the higher angles, as compared to that of the standard data NGW shown in Fig. 1(a). It is well known that the relationship of the interplanar space (d_{hkl}), diffraction angle ($\grave{e}$) and wavelength of X-ray ($\ddot{e}$) is expressed by the Bragg's equation of $2d_{hkl}$ sin $\grave{e}$ = n$\ddot{e}$. In pure NGW crystals, the unit cell decrease occurs due to the substitution of Ho^{3+} (R=1.015 Å), Yb^{3+} (R=0.985 Å) and Tm^{3+} (R=0.994 Å) ions in the Gd^{3+} (R=1.053 Å) sites [17]. According to the Bragg equation, the diffraction peaks shift to higher angles with the decrease of d_{hkl} values. To achieve a well-defined crystalline morphology of $NaGd_{0.60}(WO_4)_2:Ho_{0.04}/Yb_{0.35}/Tm_{0.01,}$ $NaGd_{0.55}(WO_4)_2:Ho_{0.03}/Yb_{0.40}/Tm_{0.02,}$ $NaGd_{0.50}(WO_4)_2:Ho_{0.02}/Yb_{0.45}/Tm_{0.03}$, and $NaGd_{0.45}(WO_4)_2:Ho_{0.01}/Yb_{0.50}/Tm_{0.04}$ particles, phases need to be heat treated at 900°C for 16 h. It is assumed that the doping amount of $Ho^{3+}/Yb^{3+}/Tm^{3+}$ has a superior effect on the crystalline cell volume of the NGW, because of the different ionic sizes. This means that the obtained samples possess a tetragonal-phase after partial substitution of Gd^{3+} by Ho^{3+}, Yb^{3+} and Tm^{3+} ions, and the ions are effectively doped into crystal lattices of the NGW phase due to the similar radii of Gd^{3+}, Ho^{3+}, Yb^{3+} and Tm^{3+}.

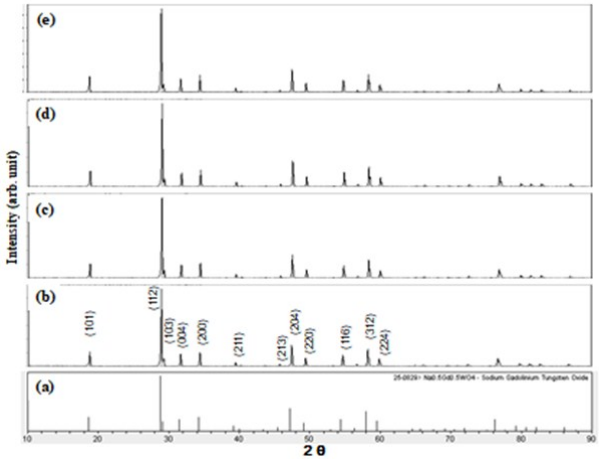

Fig. 1: XRD patterns of the (a) JCPDS 48-0886 data of NGW, the synthesized (b) $NaGd_{0.60}(WO_4)_2:Ho_{0.04}/Yb_{0.35}/Tm_{0.01,}$ (c) $NaGd_{0.55}(WO_4)_2:Ho_{0.03}/Yb_{0.40}/Tm_{0.02,}$ (d) $NaGd_{0.50}(WO_4)_2:Ho_{0.02}/Yb_{0.45}/Tm_{0.03}$, and (e) $NaGd_{0.45}(WO_4)_2:Ho_{0.01}/Yb_{0.50}/Tm_{0.04,}$ particles.

Fig. 2 shows SEM images of the synthesized (a) $NaGd_{0.60}(WO_4)_2:Ho_{0.04}/Yb_{0.35}/Tm_{0.01,}$ (b) $NaGd_{0.55}(WO_4)_2:Ho_{0.03}/Yb_{0.40}/Tm_{0.02,}$ (c) $NaGd_{0.50}(WO_4)_2:Ho_{0.02}/Yb_{0.45}/Tm_{0.03}$, and (d) $NaGd_{0.45}(WO_4)_2:Ho_{0.01}/Yb_{0.50}/Tm_{0.04}$ particles. The as-synthesized samples are very similar morphologies and no discrepancy is observed, showing superior microcrystalline morphology with particle size of 1-2 ìm. The MSG derived process of double tungstates provides unique characteristics and superior morphology for the available synthesis of UC particles.

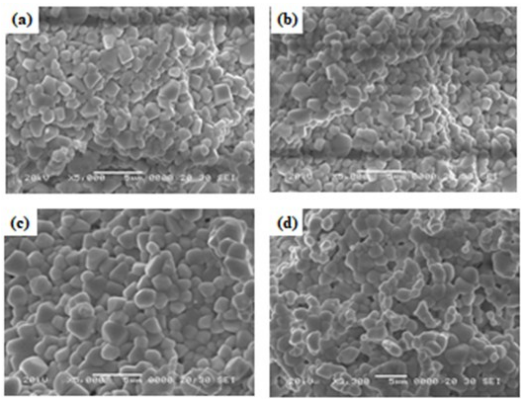

Fig. 2: SEM images of the synthesized (a) $NaGd_{0.60}(WO_4)_2:Ho_{0.04}/Yb_{0.35}/Tm_{0.01,}$ (b) $NaGd_{0.55}(WO_4)_2:Ho_{0.03}/Yb_{0.40}/Tm_{0.02,}$ (c) $NaGd_{0.50}(WO_4)_2:Ho_{0.02}/Yb_{0.45}/Tm_{0.03}$, and (d) $NaGd_{0.45}(WO_4)_2:Ho_{0.01}/Yb_{0.50}/Tm_{0.04,}$ particles.

Fig. 3 shows the UC PL emission spectra of the as-prepared (a) $NaGd_{0.60}(WO_4)_2:Ho_{0.04}/Yb_{0.35}/Tm_{0.01,}$ (b) $NaGd_{0.55}(WO_4)_2:Ho_{0.03}/Yb_{0.40}/Tm_{0.02,}$ (c) $NaGd_{0.50}(WO_4)_2:Ho_{0.02}/Yb_{0.45}/Tm_{0.03}$, and (d) $NaGd_{0.45}(WO_4)_2:Ho_{0.01}/Yb_{0.50}/Tm_{0.04}$ particles. Under excitation at 980 nm, the doped particles exhibited white emissions

based on blue, green and red emission bands, which correspond to the $^1G_4$ '! $^3H_6$ transitions of Tm^{3+} in the blue region, the $^5S_2/\ ^5F_4$ '! $^5I_8$ transitions of Ho^{3+} in the green region, the $^5F_5$ '! $^5I_8$ transitions of Ho^{3+} as well as the $^1G_4$ '! $^3F_4$ and $^3H_4$ '! $^3H_6$ transitions of Tm^{3+} in the red region. The UC intensity of (c) $NaGd_{0.50}(WO_4)_2$:$Ho_{0.02}/Yb_{0.45}/Tm_{0.03}$ exhibits the strongest 545-nm emission band in the green region and 655-nm emission band in the red region due to higher content of Tm^{3+}. However, the UC intensity of (a) $NaGd_{0.60}(WO_4)_2$:$Ho_{0.04}/Yb_{0.35}/Tm_{0.01}$ reveals the strongest 475-nm emission band in the blue region and the strongest 695-nm emission band in the red region due to higher content of Ho^{3+}. Consequently, the optimal Yb^{3+}: Ho^{3+}+Tm^{3+} ratio is as high as 9:1 for the white emitting diode based on the blue, green and red emissions.

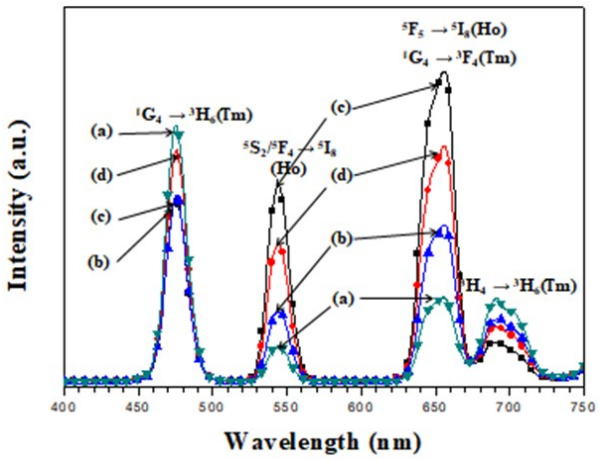

Fig. 3: UC PL emission spectra of (a) $NaGd_{0.60}(WO_4)_2$:$Ho_{0.04}/Yb_{0.35}/Tm_{0.01,}$ (b) $NaGd_{0.55}(WO_4)_2$:$Ho_{0.03}/Yb_{0.40}/Tm_{0.02,}$ (c) $NaGd_{0.50}(WO_4)_2$:$Ho_{0.02}/Yb_{0.45}/Tm_{0.03}$, and (d) $NaGd_{0.45}(WO_4)_2$:$Ho_{0.01}/Yb_{0.50}/Tm_{0.04}$ particles excited under 980 nm at room temperature.

The logarithmic scale dependence of the UC emission intensities at 475, 545, 655 and 695 nm on the working pump power over the range of 20 to 110 mW in the $NaGd_{0.50}(WO_4)_2$:$Yb_{0.02}/Ho_{0.45}/Tm_{0.03}$ sample is shown in Fig. 4. In the UC process, the UC emission intensity is proportional to the slope value *n* of the irradiation pumping power, where *n* is the number of pumped photons required to produce UC emission [18]:

$$I \propto P^n \tag{1}$$

$$\mathrm{Ln}I \propto n\mathrm{Ln}P \tag{2}$$

where value *n* is the number of the pumped photons required to excite the upper emitting state, *I* is the UC luminescent intensity and *P* is the laser pumping power. As seen from Fig. 4, the slope value calculations indicate *n* = 2.23 for blue emission at 475 nm, *n* = 1.69 for green emission at 545 nm, and *n* = 1.95 and 1.73 for red emissions at 655 and 695 nm, respectively. These results show that the UC mechanism of the blue, green and red emissions can be explained by the multi-step energy transfer process in

$Ho^{3+}/Yb^{3+}/Tm^{3+}$ tri-doped phosphors [7-9, 22-25].

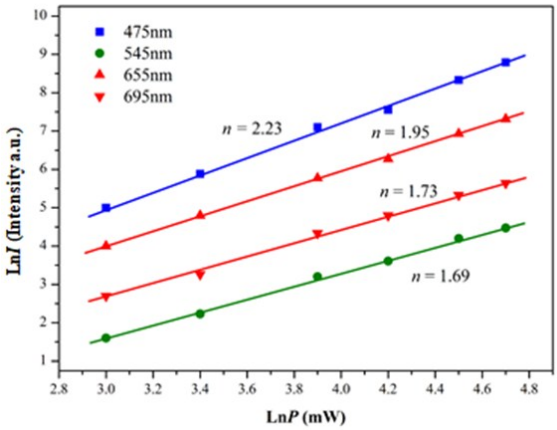

Fig. 4 : Logarithmic scale dependence of the UC emission intensity on the pump power in the range from 20 to 110 mW at 475, 545, 655 and 695 nm in the $NaGd_{0.50}(WO_4)_2:Ho_{0.02}/Yb_{0.45}/Tm_{0.03}$ sample.

For the emissions for Tm^{3+} activator, the Yb^{3+} ion sensitizer is excited from the $^2F_{7/2}$ level to the $^4F_{5/2}$ level under excitation of 980 nm pumping, and transfers its energy to Tm^{3+} ions. Then, Tm^{3+} ions is populated from the $^3H_6$ ground state to the $^3H_5$ excited state. During the phonon-assisted energy transfer process, the energy mismatch occurs between the $^2F_{5/2}$ level of Yb^{3+} and the $^3H_5$ level of Tm^{3+}. Continuously, the Tm^{3+} in the $^3H_5$ level relaxes non-radiatively to the $^3F_4$ level. The Tm^{3+} in the $^3F_4$ level is excited to the $^3F_3$ level by the energy transfer from Yb^{3+}. Furthermore, the Tm^{3+} in the $^3F_3$ relaxes also non-radiatively to the $^3H_4$ level, and is generated to the red emission of 695 nm. Subsequently, the Tm^{3+} in the $^3H_4$ level is excited to the $^1G_4$ level by the energy transfer from Yb^{3+}. Finally, the red emission at 655 nm corresponding to the $^1G_4$ '! $^3F_4$ transitions is developed, and the blue emission at 475 nm corresponding to the $^1G_4$ '! $^3H_6$ transitions is created [21,22].

Fig. 5 shows (A) calculated chromaticity coordinates (x, y) values and (B) CIE chromaticity diagram for (a) $NaGd_{0.60}(WO_4)_2:Ho_{0.04}/Yb_{0.35}/Tm_{0.01,}$ (b) $NaGd_{0.55}(WO_4)_2:Ho_{0.03}/Yb_{0.40}/Tm_{0.02,}$ (c) $NaGd_{0.50}(WO_4)_2:Ho_{0.02}/Yb_{0.45}/Tm_{0.03}$, and (d) $NaGd_{0.45}(WO_4)_2:Ho_{0.01}/Yb_{0.50}/Tm_{0.04}$ particles. The triangle depicted in Fig. 6(B) indicates standard coordinates for blue, green and red colors. The inset in Fig. 6(B) shows the chromaticity points for the samples (a), (b), (c) and (d). The chromaticity coordinates (x, y) are strongly dependent on the $Ho^{3+}/Yb^{3+}/Tm^{3+}$ concentration ratio. As indicated in Fig. 6(A), the calculated chromaticity coordinates x = 0.366 and y = 0.344 for (a) $NaGd_{0.60}(WO_4)_2:Ho_{0.04}/Yb_{0.35}/Tm_{0.01,}$ x = 0.343 and y = 0.338 for (b) $NaGd_{0.55}(WO_4)_2:Ho_{0.03}/Yb_{0.40}/Tm_{0.02,}$ x = 0.334 and y = 0.324 for (c) $NaGd_{0.50}(WO_4)_2:Ho_{0.02}/Yb_{0.45}/Tm_{0.03}$, and x = 0.332 and y = 0.318 for (d) $NaGd_{0.45}(WO_4)_2:Ho_{0.01}/Yb_{0.50}/Tm_{0.04}$ are corresponding to the standard equal energy point in CIE diagram in Fig. 6(B).

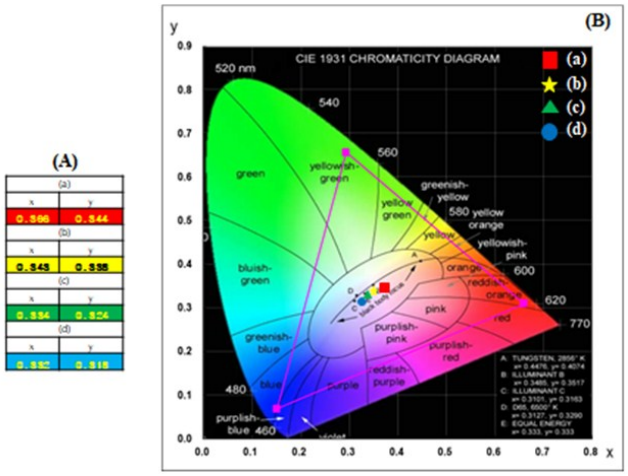

Fig. 5: (A) Calculated chromaticity coordinates (x, y) values and (B) CIE chromaticity diagram for $NaGd_{1-x}(WO_4)_2:Ho^{3+}/Yb^{3+}/Tm^{3+}$ phosphors. The inset shows the emission points for the sample synthesized (a) $NaGd_{0.60}(WO_4)_2:Ho_{0.04}/Yb_{0.35}/Tm_{0.01,}$ (b) $NaGd_{0.55}(WO_4)_2:Ho_{0.03}/Yb_{0.40}/Tm_{0.02,}$ (c) $NaGd_{0.50}(WO_4)_2:Ho_{0.02}/Yb_{0.45}/Tm_{0.03}$, and (d) $NaGd_{0.45}(WO_4)_2:Ho_{0.01}/Yb_{0.50}/Tm_{0.04,}$ particles

Fig. 6 shows the Raman spectra of the synthesized (a) pure NGW, (b) $NaGd_{0.60}(WO_4)_2:Ho_{0.04}/Yb_{0.35}/Tm_{0.01,}$ (c) $NaGd_{0.55}(WO_4)_2:Ho_{0.03}/Yb_{0.40}/Tm_{0.02,}$ (d) $NaGd_{0.50}(WO_4)_2:Ho_{0.02}/Yb_{0.45}/Tm_{0.03}$, and (e) $NaGd_{0.45}(WO_4)_2:Ho_{0.01}/Yb_{0.50}/Tm_{0.04}$ particles excited by the 514.5-nm line of an Ar ion laser at 0.5 mW. The internal modes for the (a) pure NGW particles were detected at 332, 406, 812, 880 and 918 cm^{-1}, respectively. The well-resolved sharp peaks for the NGW indicate a high crystallinity state of the synthesized particles. The internal vibration mode frequencies are dependent on the lattice parameters and the strength of the partially covalent bond between the cation and molecular ionic group WO_4. The Raman spectrum of the NGW crystal in Fig. 6(a) shows the typical tungstate compounds, which is divided into two parts with a wide empty gap of 400-800 cm^{-1} [23-25]. The stretching vibrations of W-O bonds are observed at 812 ~ 918 cm^{-1}. For these stretching vibrations, strong mixing occurs between the W-O bonds and the WO_4. The bands at 332 and 406 cm^{-1} could be assumed to originate from vibrations of the longer W-O bonds, which are employed in the formation of the W-W bridge. The translational vibration motion of the Na^{3+} ions is observed around 200 cm^{-1}, whereas the Gd^{3+} translations were located below 180 cm^{-1} [26,27]. The Raman spectra of the doped particles indicate the very strong and dominant peaks at higher frequencies of 830, 918, 1110 and 1280 cm^{-1} and at lower frequencies of 334 and 412 cm^{-1}. These strong disordered peaks at higher and lower frequencies are attributed the strong mixing between the W-O bonds and the WO_4 stretching vibrations as well as the concentration quenching effect of Ho^{3+} and Tm^{3+} ions. It is assumed that the highly modulated structure has strong absorption in the near ultraviolet region, so that energy transfer processes from the WO_{4-x} group to rare earth ions can easily occur, which can greatly enhance the external quantum efficiency of rare earth ions doped materials. These results lead to high emitting efficiency and superior thermal and chemical stability, and these materials, which can be considered potentially active components in new optoelectronic devices and in biomedical applications.

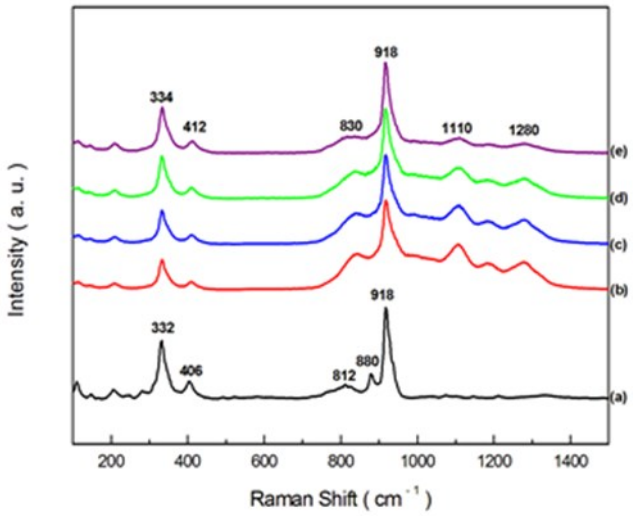

Fig. 6: Raman spectra of the synthesized (a) pure NGW, (b) $NaGd_{0.60}(WO_4)_2$:$Ho_{0.04}/Yb_{0.35}/Tm_{0.01,}$ (c) $NaGd_{0.55}(WO_4)_2$: $Ho_{0.03}/Yb_{0.40}/Tm_{0.02,}$ (d) $NaGd_{0.50}(WO_4)_2$: $Ho_{0.02}/Yb_{0.45}/Tm_{0.03}$, and (e) $NaGd_{0.45}(WO_4)_2$:$Ho_{0.01}/Yb_{0.50}/Tm_{0.04,}$ particles excited by the 514.5-nm line of an Ar ion laser at 0.5 mW.

Conclusions

The double tungstate NGW:$Ho^{3+}/Yb^{3+}/Tm^{3+}$ white phosphors were successfully synthesized by MSG derived method. The synthesized particles brought superior microcrystalline morphology with particle size of 1-2 ìm. Under excitation at 980 nm, the UC doped particles revealed white emissions based on blue, green and red emission bands, which correspond to the $^1G_4$ '! $^3H_6$ transitions of Tm^{3+} in the blue region, the $^5S_2/^5F_4$ '! $^5I_8$ transitions of Ho^{3+} in the green region, the $^5F_5$ '! $^5I_8$ transitions of Ho^{3+} as well as the $^1G_4$ '! $^3F_4$ and $^3H_4$ '! $^3H_6$ transitions of Tm^{3+} in the red region. The calculated slope value n = 2.23 for blue emission at 475 nm, n = 1.69 for green emission at 545 nm, and n = 1.95 and 1.73 for red emissions at 655 and 695 nm, respectively. The calculated chromaticity coordinates were corresponding to the standard equal energy point in CIE diagram. The strong disordered peaks at higher and lower frequencies in Raman spectroscopy were attributed the strong mixing between the W-O bonds and the WO_4 stretching vibrations as well as the concentration quenching effect of Ho^{3+} and Tm^{3+} ions. The results led to superior emitting efficiency and NGW:$Ho^{3+}/Yb^{3+}/Tm^{3+}$ white phosphors can be considered as potentially active PL materials in new optoelectronic devices and in the field of biomedical applications.

Acknowledgment

This research was supported by the Basic Science Research Program through the National Research Foundation of Korea (NRF) funded by the Ministry of Science, ICT and future Planning (2018R1D1A1A09082321).

References

[1] C.S. Lim, A. Aleksandrovsky, M. Molokeev, A. Oreshonkov, V. Atuchin, Phys. Chem. Chem. Phys., 17, 19278 (2015).

[2] M.Wang, G. Abbineni, A. Clevenger, C. Mao, S. Xu, Nanomedicine: Nanotech. Biology, and Medicine, 7, 710 (2011).

[3] C. S. Lim, A. Aleksandrovsky, M. Molokeev, A. Oreshonkov, D. Ikonnikov, V. Atuchin, Dalton Transactions, 45, 15541 (2016).

[4] L. Li, W. Zi, H. Yu, S. Gan, G. Ji, H. Zou, X. Xu, J. Lumin., 143, 14 (2013).

[5] C. Ming, F. Song, L. Yan, Opt. Comm., 286, 217 (2013).

[6] C.S. Lim, A. Aleksandrovsky, M. Molokeev, A. Oreshonkov, V. Atuchin, J. Solid State Chemistry, 228, 160 (2015).

[7] J. Jin, K. Yang, J. Su, Z. Si, J. Lumin., 159, 178 (2015).

[8] Y. Xu, Y. Wang, L. Xing, X. Tan, 54, 50 (2013).

[9] D. Li, Y. Wang, X. Zhang, G.Shi, G. Liu, Y. Song, J. Alloys Compd., 550, 509 (2013).

[10] X. Liu, W. Xiang, F. Chen, W. Zhang, Z. Hu, Mater. Res. Bull., 47, 3417 (2012).

[11] X. Liu, W. Xiang, F. Chen, Z. Hu, W. Zhang, Mater. Res. Bull., 48, 281 (2013).

[12] N. Xue, X. Fan, Z. Wang, M. Wang, Mater. Lett., 61, 1576 (2007).

[13] S. Huang, D. Wang, Y. Wang, L. Wang, X. Zhang, P. Yang, J. Alloys Compd., 529, 140 (2012).

[14] J. Feng, J. Xu, Z. Zhu, Y. Wang, Z. You, J. Li, H. Wang, C. Tu, J. Alloys Compd., 566, 229 (2013).

[15] F. Song, L. Han, H. Tan, J. Su, J. Yang, J. Tian, G. Zhang, Z. Cheng, H. Chen, Opt. Comm., 259, 179 (2006).

[16] C.S. Lim, Mater. Res. Bull., 47, 4220 (2012).

[17] R. D. Shannon, Acta Cryst., A32, 751 (1976).

[18] H. Guo, N. Dong, M. Yin, W. Zhang, L. Lou, S. Xia, J. Phys. Chem. B, 108, 19205 (2004).

[19] Y. Xu, Y. Wang, L. Shi, L. Xing, X. Tan, Opt. Laser Tech., 54, 50 (2013).

[20] X. Li, Q. Nie, S. Dai, T. Xu, L. Lu, X. Zhang, J. Alloys Compd., 454, 510 (2008).

[21] L.G.A. Carvalho, L.A. Rocha, J.M.M. Buarque, R.R. Goncalves, C.S. Nascimento Jr., M.A. Schavon, S.J.L. Ribeiro, J.L. Ferrari, J. Lumin., 159, 223 (2015).

[22] H. Gong, D. Yqang, X. Zhao, E.Y.B. Pun, H. Lim, Opt. Mater., 32, 554 (2010).

[23] T.T. Basiev, A.A. Sobel, Y.K. Voronko, P.G. Zverev, "Spontanious Raman spectroscopy of tungstate and molybdate crystals for Raman lasers," Opt. Mater., 15 [2] 205-216 (2000).

[24] V.V. Atuchin, V.G. Grossman, S.V. Adichtchev, N.V. Surovtsev, T.A. Gavrilova, B.G. Bazarov, Opt. Mater., 34, 812 (2012).

[25] A.A. Savina, V.V. Atuchin, S.F. Solodovnikov, Z.A. Solodovnikova, A.S. Krylov, E.A. Maximovskiy, M.S. Molokeev, A.S. Oreshonkov, A.M. Pugachev, E.G. Khaikina, J. Solid State Chem., 225, 53 (2015).

[26] V.V. Atuchin, O.D. Chimitova, T.A. Gavrilova, M.S. Molokeev, Sung-Jin Kim, N.V. Surovtsev, B.G. Bazarov, J. Crys. Growth, 318, 683 (2011).

[27] V.V. Atuchin, O.D. Chimitova, S.V. Adichtchev, J.G. Bazarov, T.A. Gavrilova, M.S. Molokeev, N.V. Surovtsev, Zh.G. Bazarova, Mater. Lett., 106. 26 (2013).